Chromatin state transition underlies the temporal changes in gene expression during cardiomyocyte maturation

Chia-Yeh Lin[1], Yao-Ming Chang[2], Hsin-Yi Tseng[1], Yen-Ling Shih[2], Hsiao-Hui Yeh[2], Po-Li Chen[1], Chien-Chang Chen[2], Yu-Ting Yan[2,*] and Cheng-Fu Kao[1,*]

1. Institute of Cellular and Organismic Biology, Academia Sinica, 128, Academia Road, Section 2, Nankang, Taipei, Taiwan.
2. Institute of Biomedical Sciences, Academia Sinica, 128, Academia Road, Section 2, Nankang, Taipei, Taiwan.

* Corresponding author: ckao@gate.sinica.edu.tw and yyan@ibms.sinica.edu.tw

Abstract

Congenital heart disease (CHD) is often rooted in aberrant gene expression during heart development. As cells commit to a specific lineage during development, chromatin dynamics and developmental plasticity generally become more limited. However, it remains unclear how differentiated cardiomyocytes (CMs) undergo morphological and functional adaptations to the postnatal environment during the process of CM maturation. We sought to investigate the regulatory mechanisms that control postnatal cardiac gene networks. A time-series transcriptomic analysis of postnatal hearts revealed an integrated, time-ordered transcriptional network that regulates CM maturation. Remarkably, depletion of histone H2B ubiquitin ligase RNF20 after formation of the four-chamber heart disrupted these highly coordinated gene networks. As such, its ablation caused early-onset cardiomyopathy, a phenotype reminiscent of CHD. Furthermore, the dynamic modulation of chromatin accessibility by RNF20 during CM maturation was necessary for the operative binding of cardiac transcription factors that drive transcriptional gene networks. Together, our results reveal how epigenetic-mediated chromatin state transitions modulate time-ordered gene expression for CM maturation.

Key words: RNF20, chromatin accessibility, postnatal gene networks, CM maturation

Introduction

Aberrant cellular specification during cardiogenesis may lead to congenital heart disease (CHD)[1], the most common birth defect worldwide[2], or it may lead to heart failure, a leading cause of morbidity and mortality in adult life[3]. Since precise control of gene expression is critical for heart development and maturation[4,5], knowledge of the regulatory mechanisms controlling cardiac gene networks is key to understanding the pathogenesis of cardiovascular disease.

Gene expression is tightly controlled by transcription factors (TFs) that act in accordance with epigenetic regulatory mechanisms[6,7]. TFs bind to specific sequences of DNA adjacent to a gene promoter and control its activity[6]. However, most TFs cannot access closed chromatin, and their binding to DNA relies on the presence of a permissive chromatin environment constructed by epigenetic modulators[7,8]. In heart development, epigenetic marks are established early at the embryonic stage[9,10], and dynamic changes in these marks are associated with cardiac lineage specification and stage transition[10-12].

An increasingly large body of clinical and experimental research indicates that aberrant epigenetic regulation can contribute to CHD[9,13]. For instance, alterations in histone modifying enzymes were shown to commonly occur as *de novo* mutations in CHD patients[13]. Furthermore, extensive studies have been conducted on the mechanisms by which H3K4 and H3K27 methylations impact heart development[11,14,15]. More recently, a critical role for histone H2B ubiquitylation (H2Bub) was demonstrated in cardiac development[16,17]. Knockdown of the *Xenopus* H2Bub E3 ligases, *rnf20* (Ring finger protein 20) and *rnf40* (Ring finger protein 40)[18], beginning at the two-cell stage, influences cardiac looping and left-right (LR) asymmetry during early embryonic development[16]. Furthermore, the results of an *in vivo* CRISPR/Cas9 genetic screen suggested that RNF20/40 is involved in cardiomyocyte (CM) maturation via H2Bub deposition[17]. Thus, RNF20 appears to be relevant to both CHD and CM maturation[16,19]. Nevertheless, the molecular function of RNF20 during temporal development of mammalian heart remains uncharacterized.

Dynamic regulation of the RNF20-H2Bub pathway has been linked to embryonic stem cell differentiation[20-22]. The addition of a single ubiquitin on H2B disrupts the local and higher-order structures of compacted chromatin[23,24]. This modulation of chromatin structure affects gene activities, as RNF20-H2Bub promotes the binding of TFs or regulatory proteins at gene promoters during transcription[25,26]. H2Bub is also

selectively enriched at the coding region of highly expressed genes[27], where its tight coupling with RNA polymerase II (Pol II)[25,28] and histone chaperone FACT[29] facilitate transcriptional elongation.

Results

A time-ordered transcriptional cascade during cardiomyocyte maturation

In postnatal hearts, numerous processes (cell cycle, structural, functional and metabolic transitions) are required to drive CM maturation[4,5]. These transitional processes are known to be coordinated by certain gene networks[5,30], but it remains unclear whether the transcriptional programs governing each process are regulated independently and simultaneously or by an integrated time-ordered gene network[4]; and how epigenetic mechanism might contribute to these processes. To address these open questions, we conducted two parallel time-series experiments to obtain transcriptomic data of developing hearts from P2 to P28 from control and mutant hearts of mice with the conditional ablation of *Rnf20* after cardiac morphogenesis (*Rnf20*$^{flox/flox}$*; Mck*-Cre; hereafter called *cKO*) **(Figure 1A)**. We found clearly distinctive expression profiles between all control and *cKO* pairs during CM maturation **(**PCA analysis, blue and red circles in **Figure 1B)**.

We applied the time-ordered gene coexpression network (TO-GCN) method[31] to elucidate the dynamic of developmental processes over time in control and *cKO* hearts separately **(Figure S1)**. In the analysis of control hearts, each expressed TF within the time series of transcriptomes was assigned to one of nine levels (L1 to L9) represented its expression time order over the five time-points (high expression levels are indicated by red squares in **Figure 1C and Supplementary file 1**). In the network, TFs shown at the same level indicates that they are upregulated at the same time period. Moreover, TFs displayed at consecutive levels indicates that they are upregulated in similar time orders, while TFs at lower-level are up-regulated earlier than TFs at higher-level (**Figure 1C**).

Next, we identified overrepresented functional pathways of control heart development at each level of TO-GCN by checking the corresponding coexpressed genes (**Figure 1D and Figure S1-2**). The result shows a clear time-ordered organization of transcriptional cascades to regulate CM maturation (Left panel, **Figure 1D**). For example, hypoxia-inducible factor 1 (HIF1) signaling was enriched at level 1 (L1) and quickly decreased after L2 (Left panel, **Figure 1D and S2-3**), reflecting the

transition of hypoxia to normoxia after birth[32]. Following the decrease in HIF1 signaling, most of the enriched pathways from L1 to L5 (corresponding to first week) were related to cell-cell connection, including genes supporting adherens junctions, actin cytoskeleton, tight junction focal adhesion, and ECM-receptor interaction (Left panel, **Figure 1D and Figure S2**). Genes related to cell cycle and DNA replication pathways were activated from L1/L2 (P2) to L4 (P7), reflecting a state of hyperplasia during the first week after birth [33] (Left panel, **Figure 1D**). The thyroid (T3) hormone signaling (Left panel, **Figure 1D**), required for CM growth and structural maturation [34], were enriched from L2 to L4. In addition to the upregulation of T3 signaling, we also observed sequential activation of several other signaling pathways. ErbB signaling was first activated at L2, followed by neurotrophin and PI3K-AKT signaling at L3, insulin signaling at L4 and MAPK signaling at L5 (Left panel, **Figure 1D**). The combination of ErbB and insulin signaling are thought to promote sarcomere synthesis [35,36]. Notably, cross-talk between T3 and PI3K-AKT is important for myosin heavy chain and titin isoform transitions and is critical for myocardial distensibility and mechanosignaling [37]. Furthermore, the induction of neurotrophin signaling is required for neurodevelopment and enhances normal CM Ca^{2+} cycling and contraction [38]. These enriched signaling pathways reflect cardiomyocytes undergoing structural and functional maturation (indicated by hypertrophy, isoform switch and contraction), accompanied by halting of the cell-cycle. The activated insulin signaling at L4 is important for the following fatty acid metabolism and oxidative phosphorylation at L7, reflecting a metabolism transformation in cardiomyocytes [39]. At the same time, genes involved in mitochondria biogenesis and organization were highly expressed (**Figure S2**), consistent with idea that maturing CMs undergo a transition of primary energy source from glucose to fatty acids [40]. Lastly, the pathway of cardiac muscle contraction was enhanced at L8 (P21) (Left panel, **Figure 1D and Figure S2**), in line with enhanced heart function at this stage. In summary, the analysis revealed an integrated, time-ordered transcriptional network that accurately reflects the known coordination of signaling cascades regulating CM maturation in the first three weeks of life.

Coordinated gene networks is critical for postnatal CM development

Compared to the results in control hearts, we observed drastically different transcriptional regulatory cascades in *cKO* hearts (**Figure 1D and S3**). The disturbance by *Rnf20* deletion could be observed as early as at L1 (corresponding to P2). For

example, the HIF-1 signaling pathway were enriched at L1 and L9 in control and *cKO* hearts, respectively. Intriguingly, the most dramatically dysregulated pathways at L1 in *cKO* hearts are related to actin cytoskeleton, tight junctions and adherens junctions, which contribute to myocyte-myocyte communication[41] and regulate cell shape (**Figure 1D and Figure S2**). In addition, delay of ErbB signaling and disruptions in many metabolic networks (i.e., inactivation of fructose/mannose, propanoate and 2-oxocarboxylic acid metabolism, and the early activation of fatty acid metabolism) were also observed in c*KO* (**Figure 1D**). These disruptions were reflected by the inactivation of genes involved in mitochondria biogenesis (**Figure S2**). Thus, RNF20 is critical for the coordination of gene networks during CM maturation, as early as the initial postnatal response to the hypoxia-to-normoxia shift.

Ablation of *Rnf20* after chamber formation leads to dilated cardiomyopathy

Mck-Cre ablated *Rnf20* in cardiac and skeletal muscle cells at E13.5[42] (**Figure 2A and S4**). The ablation of *Rnf20* by *Mck-Cre* did not affect the Mendelian ratio of each genotype at postnatal day 1 (P1) (**Table S1**). However, compared to other littermates, *cKO* mice showed significantly lower body weight and sudden death beginning at P35 (**Figure 2B and 2C**). Strikingly, all *cKO* mice died within 8 weeks (P56) of birth (**Figure 2C**). At birth, both the control (*flox/flox*) and *cKO* mice had hearts with normal structures, and as expected, the cardiac sizes increased with time (**Figure 2D**). However, the *cKO* hearts developed a pronounced ventricular chamber dilation after P28 **(Figure 2D)**. Echocardiographic analysis revealed that the left ventricle (LV) systolic function, as measured by fractional shortening (FS) and ejection fraction (EF), was significantly impaired after P28 **(Figure 2E)**. We also detected abnormal electrocardiogram (ECG) patterns in *cKO* mice beginning at P14 **(Figure 2F)**. The depolarization and repolarization of the *cKO* ventricles were disturbed, exhibiting prolonged QRS complex and QT interval **(Figure 2F)**. ECG also revealed that the *cKO* mice developed irregular heartbeat at P28 **(Figure S5)**. Thus, the *cKO* mice appear to suffer from dilated cardiomyopathy[43] and arrhythmia, which may cause their sudden death.

Notably, deletion of Rnf20 before chamber formation is embryonic lethal as no liveborn *Rnf20*$^{flox/flox}$; *Mesp1-Cre* mice were recovered (**Table S2**), and the mutant embryos displayed a heart looping defect at E9.5, growth retardation at E10.5 and were absorbed before E12.5 (**Figure 2A and S6**). *Mesp1-Cre* is activated at embryonic day 6.5 (E6.5)[44]; thus, the lack of RNF20 before chamber formation (E10-13.5 in mice)

prevents proper heart morphogenesis. Furthermore, these cardiac defects were not general effects of myopathy since mice with muscle-specific knockout of *Rnf20* (*Rnf20*$^{flox/flox}$*; Hsa-Cre*)[45] exhibited identical growth curves, survival rates, heart morphologies and cardiac functions to control mice at P49 (**Figure S7**). Taken together, these findings lead us to conclude that RNF20-mediated transcriptional network is essential for postnatal cardiac development and function.

Structural, functional and metabolic transitions in postnatal heart

Since the results up to this point implied that lack of RNF20 may disrupt multiple processes in CM maturation, we sought to analyze the biological outcomes of *Rnf20 cKO* in mouse heart. We first tested whether the loss of RNF20 affects the polarization of intercalated discs (IDs), a hallmark of structural maturation of CM[5,30] (**Figure 3A**). The major components of IDs include N-cadherin (an adherens junction protein), connexin 43 (a gap junction protein) and desmoplakin (a cytoplasmic desmosomal protein). These components were circumferentially distributed at P2 and gradually became polarized (P21), migrating to the ends of the cardiomyocytes at P35 in the control hearts (**Figure 3B and S8A-B**). In contrast, the migration was completely abolished in the CMs of *cKO* mice. Next, we characterized the ultrastructure changes in IDs during CM maturation using transmission electron microscopy (TEM). IDs were visible and adjacent to the intercellular space between myocytes in the control cardiomyocytes at P21 and P35, with clear adherent junctions (white arrow in **Figure 3C**) and desmosomes (yellow arrow in **Figure 3C**). By contrast, the structures of IDs in mutant hearts were fragmented and disorganized (P21). By P35, the IDs were even degenerated with widened gaps.

The structural maturation of cardiomyocytes (**Figure 3D**) may also be assessed by the localization of vinculin, a membrane-cytoskeletal protein controlling cytoskeletal mechanics and cell shape[46] (**Figure 3E**). In the control mouse myocardium, cytoplasmic vinculin migrated to the cell membrane during maturation (upper panel, **Figure 3E**); however, the majority of vinculin remained in the cytoplasmic region in RNF20-depleted mutants (lower panel, **Figure 3E**). Furthermore, we found that the cardiomyocytes in *cKO* mice failed to adopt a rectangular shape at P35 **(Figure 3E and S8C)**. Since CM cell shape is intimately linked to sarcomere alignment[47], we also inspected the myofibril organization in postnatal hearts by TEM (**Figure 3F**). In contrast to the control group, the myofibril alignment in cardiomyocytes of *cKO* was

219 distorted, exhibiting loose actin filaments (yellow arrow in **Figure 3F**) and fuzzy Z-
220 lines (white arrowhead in **Figure 3F**); the M-line was also difficult to distinguish
221 (yellow arrowhead in **Figure 3F**).

222 Last, we examined the effects of *Rnf20 cKO* on CM metabolic maturation, as
223 indicated by the maturation of mitochondria (**Figure 3G**)[4,5]. Control hearts showed a
224 gradual morphological shift from small, tubular and round mitochondria to large, ovoid,
225 well-organized organelles between P7 and P35 (**Figure 3H and S8D**), which is typical
226 of developing hearts[30]. However, this morphological maturation did not occur in
227 mitochondria of *cKO* hearts (**Figure 3H and S8D**). We next analyzed the arrangement
228 and density of cristae by TEM. Interestingly, the arrangement of cristae was not altered
229 in *cKO* mutants. However, a breakdown of both inner and outer membrane was
230 observed at postnatal day 35 (*cKO* in **Figure 3H**). Furthermore, mitochondria cristae
231 density (an indicator of mitochondria function)[5] was low from P21 onwards in *cKO*
232 hearts (**Figure 3H**). The mitochondria DNA (mtDNA) copy number was reduced by
233 20% at P35 in *cKO* mice (**Figure S7E**). In addition, the protein levels of major electron
234 transport chain components, cytochrome c oxidase and COX VI were markedly
235 decreased in mutant heart (**Figure 3I**). The observed low enzyme activities of
236 cytochrome c oxidase (**Figure 3J**) and NADH oxidase (**Figure 3K**)[48] were likely
237 responsible for the drastic reduction of ATP in *cKO* myocardium (**Figure 3L**).
238 Collectively, these data suggested that RNF20 extensively regulates CM maturation by
239 orchestrating gene networks and their functional outcomes.
240
241 **The dynamic chromatin opening during CM maturation**
242 Since RNF20 is known to be an epigenetic factor that modulates chromatin
243 compaction via monoubiquitylating histone H2B[23], we wondered whether Rnf20-
244 mediated epigenetic landscaping is involved in regulating the transcriptional networks
245 during postnatal CM development **(Figure 1D)**. To this end, we profiled the chromatin
246 accessibility by ATAC-seq[49] in postnatal hearts of two time points, P7 and P21 (**Figure**
247 **4A**), which represented the early and late stages, respectively, of the postnatal
248 transcriptional maturation programs. In control hearts, we found the number of wide-
249 spread accessible regions (peaks) reduced by almost 50% at P21 against P7 (**Figure**
250 **4B**). Most of reduced peaks were from promoter regions (from 13,320 to 3,714 peaks;
251 reduction of 72.1%; **Figure 4B and supplementary file 2**). Intriguingly, this dynamic
252 change in chromatin accessibility was positively correlated to the level of RNF20 in

control hearts (**Figure 4C**), suggesting that the chromatin in early and late stages displayed distinctive epigenetic landscapes.

On the other hand, we found only about a half of peaks were detected in the genome of P7 in *cKO* hearts. Compared to P7 of control, number of detected peaks decreased in all genomic regions but predominantly in promoter regions (from 13,320 to 5,567 peaks; reduction of 58.2%; **Figure 4B**). These results suggest that RNF20 facilitates chromatin accessibility, especially during the early stage of postnatal heart development.

Promoter-opening is required for postnatal gene expression

Since the loss of *Rnf20* primarily impacted accessibility at gene promoters and nucleosome eviction at gene promoter is one of the major events during transcriptional activation[50], we postulated that RNF20-mediated chromatin opening may affect postnatal transcriptional regulation. To test this hypothesis, we identified genes with ATAC-seq peaks within 3Kb of the transcription starting sites (TSS) (**Figure 4D**). A large number of peak-associated genes (11,543 genes) was identified in the control hearts at P7, while only 6,425 genes were associated with accessible promoters in P7 *cKO* hearts (**Figure 4D**). This indicated that almost fifty percent (49.5%; 5,713) of active genes in the P7 heart may require RNF20 for their promoter opening; such genes are hereafter called "RNF20-open" genes (**Figure 4D**). KEGG pathway enrichment analysis shows that "RNF20-open" genes were enriched in pathways related to CM maturation, such as calcium signaling, cell cycle, fatty acid metabolism, gap junction, and thyroid hormone synthesis[4,5] (**Figure S10**). Only a small fraction of genes (595 genes) was classified as "*cKO*-open" genes (**Figure 4D**), indicating their promoters were accessible under RNF20 depletion. These genes showed no apparent functional links with heart development (**Figure S10**). These findings revealed that RNF20-mediated chromatin opening at P7 regulates transcriptional programs in CM maturation and thus may play a critical role in coordinating postnatal gene networks.

At P21, the number of peak-associated genes in the control hearts was comparable to that in the *cKO* hearts (5,288 in the control and 5,108 in *cKO*). However, the genes in these two groups overlapped by only about 50% (**Figure 4D**), and there were roughly equal numbers of "RNF20-open" (2646) and "*cKO*-open" (2466) genes. Of note, the "RNF20-open" genes were involved in metabolism-related pathways, such as pyruvate metabolism, glucagon signaling, regulation of lipolysis in adipocytes (**Figure S11**).

These RNF20-associated pathways mostly correlated with enriched functions at the later stages of CM maturation (**Figure 1D and S3**). In contrast, the "*cKO*-open" genes were enriched in Wnt signaling pathway, ECM-receptor interaction and neurotrophin signaling (**Figure S11**), which were highly expressed at the neonatal phase (P2 to P7) (**Figure 1D**). Thus, the ablation of *Rnf20* causes the transcriptional program of P21 heart to retain similarity with the initial postnatal stage and impairs CM maturation.

Chromatin remodeling facilitates dynamic binding of TFs during postnatal heart development

Previous studies reported that gene network transitions during heart development are tightly controlled by TFs[51], we were wondering whether RNF20-mediated changes in chromatin accessibility affect the binding of TFs to modulate postnatal heart development. To this end, we used a computational tool, TOBIAS[52] to perform a TF footprint analysis with the ATAC-seq data (**Figure 4E**). In the result, differential binding scores (DBSs) of 746 TFs represent their relative binding efficiency between the control and *cKO* groups (**Figure 4F**; a full list of analyzed TFs can be found in **Supplementary file 3**). For P7, we identified 199 RNF20-dependent and 39 *cKO*-dependent TFs by their binding activity ($-\log_{10}$p-value > 100) in the control (DBS > 0.25) and *cKO* (DBS < -0.25) groups, respectively (**Figure 4F and supplementary file 3**). Gene Ontology (GO) enrichment analysis shows that the RNF20-dependent TFs were involved in cardiac development and CM maturation (**Figure 4F and S12A**). Remarkably, many of the RNF20-dependent TFs at P7 turned to be *cKO*-dependent (DBS < 0) at P21 (**Figure 4F**), which is in line with the chromatin opening profile in the *cKO* hearts (p21 in **Figure 4D**). These results provide further explanation for the extensive transcriptional dysregulation caused by deletion of *Rnf20* (**Figure 2D**). Conversely, the binding patterns of the 39 *cKO*-dependent TFs became sparsely distributed, and their functional categories were unrelated to heart development/function (**Figure 4F and S12B**). Taken together, these observations suggest that the elevated levels of RNF20 at the early stage (P7) of CM maturation are necessary for proper binding of cardiac TFs that drive transcriptional gene networks, and the continual expression of RNF20 at lower levels is required to sustain gene-network transitions (**Figure 4G)**. Thus, RNF20 is centrally involved in establishing a dynamic epigenetic environment that facilitates the execution of time-ordered gene networks during postnatal heart development (**Figure 1D)**.

Pioneer factors contribute to chromatin opening

Of note, almost 50% of genes in the control hearts of P7 (50.5%, 5830 genes) and P21 (46.44%, 2642 genes) did not require RNF20 for promoter opening **(Figure 4D)**: defined as "persistent-open" genes. The products of "persistent-open" genes included the regulatory factors that are essential for CM maturation, such as HIF-1 signaling, ErbB signaling pathway and tight junction (**Figure 1D, S10 and S11**), suggesting there must be other factors required to maintain the basal level of chromatin opening which governs these maturation functions. It is interesting that many pioneer factors, including GATA families (GATA4, GATA6) and forkhead box families (FOXA1, FOXA2) (yellow dots in **Figure 4F**), did not rely on RNF20 for recognition site binding [low Dbs (x-axis) and low p-value (y-axis); **Supplementary file 3**]. Pioneer factors are able to open closed chromatin sites in order to implement cell fate programs[53]. Consistent with their pioneering roles during embryonic heart development[54,55], expression levels of GATA4 and GATA6 were high at early postnatal stages (L1-L2 by TO-GCN analysis, **Figure 2C**). Thus, the promoter accessibilities of "persistent-open" genes are likely attributable to the cooperation of pioneer factors via RNF20-independent mechanisms. Intriguingly, the time-ordered expression of some "persistent-open" genes were disrupted in the absence of RNF20 (**Figure 1D, S10 and S11**). As such, RNF20 may also regulate the optimal expression of "persistent-open" genes in postnatal heart without affecting the chromatin accessibility at their promoters.

Discussion

In this study, we found that RNF20-dependent modulation of dynamic chromatin accessibility is required for the time-ordered transcription of postnatal genes and CM maturation. Our analyses demonstrated that the epigenetic factor, RNF20 is essential for heart specification and morphogenesis at early stages; then, it is also required for CM adaptation to body size and workload during postnatal growth (**Figure 5A**). We further identified a transcriptional regulatory cascade that orchestrates the sequential structural, cell-cycle, functional and metabolic maturation programs in the postnatal heart (**Figure 5B**). Evidence from our study suggests that RNF20 plays a key role in regulating the time-ordered gene networks during postnatal CM maturation by modulating chromatin accessibility. Mechanistically, RNF20-mediated chromatin opening in the early postnatal heart globally resolves epigenetic barriers to allow the

maturation program to proceed. The decrease of RNF20 expression at the end-stage of maturation then reestablishes a more compact epigenetic state with less transcriptional flexibility, which is required for the mature cells. RNF20 is likely to modulate chromatin accessibility through its epigenetic target, H2Bub [29], as this modification has been shown to disrupt local and higher-order chromatin compaction *in vitro* and *in vivo* [23,24]. However, our data do not exclude the possibility that RNF20 may regulate other epigenetic factors to affect the postnatal chromatin landscape.

Global differences in chromatin accessibility have been observed during development of several different species, such as humans and flies [56,57]. Accessibility of chromatin may also differ across different life stages, as demonstrated in the developing and aged *C. elegans* [58]. Stage-specific reorganization of the chromatin landscape in cells also appears to be critical for lineage-specific gene expression, highlighting the importance of chromatin accessibility in cell-fate determination [59]. The dynamics of chromatin accessibility are modulated by the combined effects of chromatin remodelers[60,61], TFs[62] and PTMs[63]. However, it remains uncertain how accessibility of chromatin is modulated in response to external stimuli and developmental cues. Overwhelming evidence supports the roles of different PTMs in generating functional chromatin states[64], and PTMs are known to influence chromatin accessibility via indirect mechanisms, such as altering TF binding and nucleosome affinity of chromatin remodelers. Intriguingly, however, uncertainty remains about how PTMs may directly contribute to accessibility remodeling of chromatin templates. Our finding that RNF20 helps to establish a dynamic chromatin environment for CM maturation has some intriguing implications. First, the deletion of *Rnf20* after cardiac morphogenesis does not change cell fates or identity during prenatal or neonatal heart development, but it dramatically compromises CM maturation. At the molecular level, we found that RNF20 influences chromatin opening in nearly half of the gene promoters involved in CM maturation, suggesting that there is a division of labor for modulating chromatin accessibility. The cardiac-specific pioneer factors most likely specialize in modulating the chromatin states in those parts of the genome required for cardiac cell fate. In contrast, RNF20 (possibly via H2Bub) may promote chromatin plasticity in the rest of genome, allowing the heart cells to undergo remodeling from a fetal to an adult state without affecting core cell identity factors. Thus, our findings suggest a novel mechanism in which PTMs directly and extensively modulate chromatin accessibility dynamics to orchestrate developmental processes.

The mechanisms of regulating and coordinating constituent processes during CM maturation have received increasing attention because it is not yet possible to achieve complete maturation of pluripotent stem cell (PSC)-induced CMs (iPSC-CMs)[4]. Our TO-GCN analysis revealed that postnatal heart development is initiated by integrated signals, including transient expression of hypoxia-inducible factor 1-alpha (HIF-1α), cell-cell connection (adherens and tight junction) and structural organization (regulation of actin cytoskeleton). Thus, the coordinated activation of these pathways may help initiate CM maturation. In support of this idea, the synergistic application of electrical/mechanical stimulation, extracellular matrix and non-CM co-cultures can facilitate iPSC-CMs maturation[30,65]. Furthermore, the inhibition of HIF1α enhances the contractile, electrophysiologic and metabolic maturation of iPSC-CMs [66,67]. The maturation of CMs involves a complex transcriptional network coordinated by cardiac and non-cardiac cells[30,41,68-70]. Our study provides clear staging information and delineation of transcriptionally active maturation processes based on analyses of whole heart transcriptomes using a comparative transcriptomic method[31]. Thus, our approach may serve to identify the complete set of processes underlying CM maturation. Furthermore, our mouse genetic results imply that RNF20 mutations may cause CHD, as supported by previous observations in CHD patients and in *Xenopus*[13,16]. The results further suggest that functional RNF20 abnormalities beginning at late-gestation periods could be related to early-onset cardiomyopathy in children and young adults, even without observable effects on heart morphogenesis.

In summary, our findings demonstrate that dynamic chromatin accessibility is critical for the time-ordered expression of postnatal genes during CM maturation, and the epigenetic factor RNF20 plays a decisive role in mediating postnatal chromatin accessibility remodeling. We also offer a complete roadmap of gene cascades that direct CM maturation, providing insights that may improve therapies for CHD and facilitate the development of iPSC-CMs to treat heart disease.

Acknowledgments

The authors thank Dr. Ting-Fen Tsai for constructive comments during manuscript preparation. We are grateful to the staff at the Core Facility of the Institute of Cellular and Organismic Biology, Academia Sinica, for EM service and confocal assistance; the Transgenic Core Facility of the Institute of Molecular Biology, Academia Sinica, for

transgenic mice production and Genomics core facility of the Institute of Molecular Biology, Academia Sinica, for NGS service. The authors also thank the Taiwan Mouse Clinic, Academia Sinica, and Taiwan Animal Consortium for the technical support in electrocardiography and high-frequency ultrasound, and Dr. Marcus Calkins for English editing. This work was supported by the intramural funding of the Institute of Cellular and Organismic Biology, Academia Sinica, and by grants from the Ministry of Science and Technology, Taiwan (MOST 109-2320-B-001-017-MY3).

Supplementary information

Experimental designs, materials, additional information and references are available in the supplemented files.

References

1 Epstein, J. A. Franklin H. Epstein Lecture. Cardiac development and implications for heart disease. *N Engl J Med* **363**, 1638-1647, doi:10.1056/NEJMra1003941 (2010).

2 Hoffman, J. I. & Kaplan, S. The incidence of congenital heart disease. *J Am Coll Cardiol* **39**, 1890-1900, doi:10.1016/s0735-1097(02)01886-7 (2002).

3 McMurray, J. J. Clinical practice. Systolic heart failure. *N Engl J Med* **362**, 228-238, doi:10.1056/NEJMcp0909392 (2010).

4 Kannan, S. & Kwon, C. Regulation of cardiomyocyte maturation during critical perinatal window. *J Physiol* **598**, 2941-2956, doi:10.1113/JP276754 (2020).

5 Guo, Y. & Pu, W. T. Cardiomyocyte Maturation: New Phase in Development. *Circ Res* **126**, 1086-1106, doi:10.1161/CIRCRESAHA.119.315862 (2020).

6 Latchman, D. S. Transcription factors: an overview. *Int J Biochem Cell Biol* **29**, 1305-1312, doi:10.1016/s1357-2725(97)00085-x (1997).

7 Liu, L., Jin, G. & Zhou, X. Modeling the relationship of epigenetic modifications to transcription factor binding. *Nucleic Acids Res* **43**, 3873-3885, doi:10.1093/nar/gkv255 (2015).

8 Bannister, A. J. & Kouzarides, T. Regulation of chromatin by histone modifications. *Cell Res* **21**, 381-395, doi:10.1038/cr.2011.22 (2011).

9 Jarrell, D. K., Lennon, M. L. & Jacot, J. G. Epigenetics and Mechanobiology in Heart Development and Congenital Heart Disease. *Diseases* **7**, doi:10.3390/diseases7030052 (2019).

10 Paige, S. L. *et al.* A temporal chromatin signature in human embryonic stem cells identifies regulators of cardiac development. *Cell* **151**, 221-232, doi:10.1016/j.cell.2012.08.027 (2012).

11 Wamstad, J. A. *et al.* Dynamic and coordinated epigenetic regulation of developmental transitions in the cardiac lineage. *Cell* **151**, 206-220,

doi:10.1016/j.cell.2012.07.035 (2012).

12 Gilsbach, R. *et al.* Dynamic DNA methylation orchestrates cardiomyocyte development, maturation and disease. *Nat Commun* **5**, 5288, doi:10.1038/ncomms6288 (2014).

13 Zaidi, S. *et al.* De novo mutations in histone-modifying genes in congenital heart disease. *Nature* **498**, 220-+, doi:10.1038/nature12141 (2013).

14 Ang, S. Y. *et al.* KMT2D regulates specific programs in heart development via histone H3 lysine 4 di-methylation. *Development* **143**, 810-821, doi:10.1242/dev.132688 (2016).

15 Wan, X. *et al.* Mll2 controls cardiac lineage differentiation of mouse embryonic stem cells by promoting H3K4me3 deposition at cardiac-specific genes. *Stem Cell Rev Rep* **10**, 643-652, doi:10.1007/s12015-014-9527-y (2014).

16 Robson, A. *et al.* Histone H2B monoubiquitination regulates heart development via epigenetic control of cilia motility. *Proc Natl Acad Sci U S A* **116**, 14049-14054, doi:10.1073/pnas.1808341116 (2019).

17 VanDusen, N. J. *et al.* Massively parallel in vivo CRISPR screening identifies RNF20/40 as epigenetic regulators of cardiomyocyte maturation. *Nat Commun* **12**, 4442, doi:10.1038/s41467-021-24743-z (2021).

18 Fuchs, G. & Oren, M. Writing and reading H2B monoubiquitylation. *Biochim Biophys Acta* **1839**, 694-701, doi:10.1016/j.bbagrm.2014.01.002 (2014).

19 VanDusen, N. J. *et al.* Massively parallel in vivo CRISPR screening identifies RNF20/40 as epigenetic regulators of cardiomyocyte maturation. *Nat Commun* **12**, 4442, doi:10.1038/s41467-021-24743-z (2021).

20 Chen, S., Li, J., Wang, D. L. & Sun, F. L. Histone H2B lysine 120 monoubiquitination is required for embryonic stem cell differentiation. *Cell Res* **22**, 1402-1405, doi:10.1038/cr.2012.114 (2012).

21 Fuchs, G. *et al.* RNF20 and USP44 regulate stem cell differentiation by modulating H2B monoubiquitylation. *Mol Cell* **46**, 662-673, doi:10.1016/j.molcel.2012.05.023 (2012).

22 Karpiuk, O. *et al.* The histone H2B monoubiquitination regulatory pathway is required for differentiation of multipotent stem cells. *Mol Cell* **46**, 705-713, doi:10.1016/j.molcel.2012.05.022 (2012).

23 Fierz, B. *et al.* Histone H2B ubiquitylation disrupts local and higher-order chromatin compaction. *Nat Chem Biol* **7**, 113-119, doi:10.1038/nchembio.501 (2011).

24 Moyal, L. *et al.* Requirement of ATM-dependent monoubiquitylation of histone H2B for timely repair of DNA double-strand breaks. *Mol Cell* **41**, 529-542, doi:10.1016/j.molcel.2011.02.015 (2011).

25 Zhang, F. & Yu, X. WAC, a functional partner of RNF20/40, regulates histone H2B ubiquitination and gene transcription. *Mol Cell* **41**, 384-397, doi:10.1016/j.molcel.2011.01.024 (2011).

26 Kim, J., Hake, S. B. & Roeder, R. G. The human homolog of yeast BRE1 functions as a transcriptional coactivator through direct activator interactions. *Mol Cell* **20**, 759-770, doi:10.1016/j.molcel.2005.11.012 (2005).

27 Minsky, N. *et al.* Monoubiquitinated H2B is associated with the transcribed region of highly expressed genes in human cells. *Nat Cell Biol* **10**, 483-488, doi:10.1038/ncb1712 (2008).

28 Xiao, T. *et al.* Histone H2B ubiquitylation is associated with elongating RNA polymerase II. *Mol Cell Biol* **25**, 637-651, doi:10.1128/MCB.25.2.637-651.2005 (2005).

29 Pavri, R. *et al.* Histone H2B monoubiquitination functions cooperatively with FACT to regulate elongation by RNA polymerase II. *Cell* **125**, 703-717, doi:10.1016/j.cell.2006.04.029 (2006).

30 Karbassi, E. *et al.* Cardiomyocyte maturation: advances in knowledge and implications for regenerative medicine. *Nat Rev Cardiol* **17**, 341-359, doi:10.1038/s41569-019-0331-x (2020).

31 Chang, Y. M. *et al.* Comparative transcriptomics method to infer gene coexpression networks and its applications to maize and rice leaf transcriptomes. *Proceedings of the National Academy of Sciences of the United States of America* **116**, 3091-3099, doi:10.1073/pnas.1817621116 (2019).

32 Semenza, G. L. Hydroxylation of HIF-1: oxygen sensing at the molecular level. *Physiology (Bethesda)* **19**, 176-182, doi:10.1152/physiol.00001.2004 (2004).

33 Porrello, E. R. *et al.* Transient regenerative potential of the neonatal mouse heart. *Science* **331**, 1078-1080, doi:10.1126/science.1200708 (2011).

34 Grais, I. M. & Sowers, J. R. Thyroid and the heart. *Am J Med* **127**, 691-698, doi:10.1016/j.amjmed.2014.03.009 (2014).

35 Sanchez-Soria, P. & Camenisch, T. D. ErbB signaling in cardiac development and disease. *Semin Cell Dev Biol* **21**, 929-935, doi:10.1016/j.semcdb.2010.09.011 (2010).

36 Bertrand, L., Horman, S., Beauloye, C. & Vanoverschelde, J. L. Insulin signalling in the heart. *Cardiovasc Res* **79**, 238-248, doi:10.1093/cvr/cvn093 (2008).

37 Kruger, M. *et al.* Thyroid hormone regulates developmental titin isoform transitions via the phosphatidylinositol-3-kinase/ AKT pathway. *Circ Res* **102**, 439-447, doi:10.1161/CIRCRESAHA.107.162719 (2008).

38 Feng, N. *et al.* Constitutive BDNF/TrkB signaling is required for normal cardiac

contraction and relaxation. *Proc Natl Acad Sci U S A* **112**, 1880-1885, doi:10.1073/pnas.1417949112 (2015).

39 Riehle, C. & Abel, E. D. Insulin Signaling and Heart Failure. *Circ Res* **118**, 1151-1169, doi:10.1161/CIRCRESAHA.116.306206 (2016).

40 Lopaschuk, G. D. & Jaswal, J. S. Energy metabolic phenotype of the cardiomyocyte during development, differentiation, and postnatal maturation. *J Cardiovasc Pharmacol* **56**, 130-140, doi:10.1097/FJC.0b013e3181e74a14 (2010).

41 Tirziu, D., Giordano, F. J. & Simons, M. Cell communications in the heart. *Circulation* **122**, 928-937, doi:10.1161/CIRCULATIONAHA.108.847731 (2010).

42 Johnson, J. E., Wold, B. J. & Hauschka, S. D. Muscle Creatine-Kinase Sequence Elements Regulating Skeletal and Cardiac-Muscle Expression in Transgenic Mice. *Molecular and Cellular Biology* **9**, 3393-3399, doi:Doi 10.1128/Mcb.9.8.3393 (1989).

43 Japp, A. G., Gulati, A., Cook, S. A., Cowie, M. R. & Prasad, S. K. The Diagnosis and Evaluation of Dilated Cardiomyopathy. *J Am Coll Cardiol* **67**, 2996-3010, doi:10.1016/j.jacc.2016.03.590 (2016).

44 Saga, Y. *et al.* MesP1: a novel basic helix-loop-helix protein expressed in the nascent mesodermal cells during mouse gastrulation. *Development* **122**, 2769-2778 (1996).

45 Miniou, P. *et al.* Gene targeting restricted to mouse striated muscle lineage. *Nucleic Acids Res* **27**, e27, doi:10.1093/nar/27.19.e27 (1999).

46 Goldmann, W. H. & Ingber, D. E. Intact vinculin protein is required for control of cell shape, cell mechanics, and rac-dependent lamellipodia formation. *Biochem Biophys Res Commun* **290**, 749-755, doi:10.1006/bbrc.2001.6243 (2002).

47 Bray, M. A., Sheehy, S. P. & Parker, K. K. Sarcomere alignment is regulated by myocyte shape. *Cell Motil Cytoskeleton* **65**, 641-651, doi:10.1002/cm.20290 (2008).

48 Anraku, Y. Bacterial electron transport chains. *Annu Rev Biochem* **57**, 101-132, doi:10.1146/annurev.bi.57.070188.000533 (1988).

49 Corces, M. R. *et al.* An improved ATAC-seq protocol reduces background and enables interrogation of frozen tissues. *Nat Methods* **14**, 959-962, doi:10.1038/nmeth.4396 (2017).

50 John, S. *et al.* Chromatin accessibility pre-determines glucocorticoid receptor binding patterns. *Nat Genet* **43**, 264-268, doi:10.1038/ng.759 (2011).

51 Uosaki, H. *et al.* Transcriptional Landscape of Cardiomyocyte Maturation. *Cell*

Rep **13**, 1705-1716, doi:10.1016/j.celrep.2015.10.032 (2015).

52 Bentsen, M. *et al.* ATAC-seq footprinting unravels kinetics of transcription factor binding during zygotic genome activation. *Nat Commun* **11**, 4267, doi:10.1038/s41467-020-18035-1 (2020).

53 Iwafuchi-Doi, M. & Zaret, K. S. Pioneer transcription factors in cell reprogramming. *Genes Dev* **28**, 2679-2692, doi:10.1101/gad.253443.114 (2014).

54 Sharma, A. *et al.* GATA6 mutations in hiPSCs inform mechanisms for maldevelopment of the heart, pancreas, and diaphragm. *Elife* **9**, doi:10.7554/eLife.53278 (2020).

55 Tremblay, M., Sanchez-Ferras, O. & Bouchard, M. GATA transcription factors in development and disease. *Development* **145**, doi:10.1242/dev.164384 (2018).

56 Liu, L. *et al.* An integrated chromatin accessibility and transcriptome landscape of human pre-implantation embryos. *Nat Commun* **10**, 364, doi:10.1038/s41467-018-08244-0 (2019).

57 Thomas, S. *et al.* Dynamic reprogramming of chromatin accessibility during Drosophila embryo development. *Genome Biol* **12**, R43, doi:10.1186/gb-2011-12-5-r43 (2011).

58 Janes, J. *et al.* Chromatin accessibility dynamics across C. elegans development and ageing. *Elife* **7**, doi:10.7554/eLife.37344 (2018).

59 Li, D., Shu, X., Zhu, P. & Pei, D. Chromatin accessibility dynamics during cell fate reprogramming. *EMBO Rep* **22**, e51644, doi:10.15252/embr.202051644 (2021).

60 Iurlaro, M. *et al.* Mammalian SWI/SNF continuously restores local accessibility to chromatin. *Nat Genet* **53**, 279-287, doi:10.1038/s41588-020-00768-w (2021).

61 Schick, S. *et al.* Acute BAF perturbation causes immediate changes in chromatin accessibility. *Nat Genet* **53**, 269-278, doi:10.1038/s41588-021-00777-3 (2021).

62 Klemm, S. L., Shipony, Z. & Greenleaf, W. J. Chromatin accessibility and the regulatory epigenome. *Nat Rev Genet* **20**, 207-220, doi:10.1038/s41576-018-0089-8 (2019).

63 Allis, C. D. & Jenuwein, T. The molecular hallmarks of epigenetic control. *Nat Rev Genet* **17**, 487-500, doi:10.1038/nrg.2016.59 (2016).

64 Ernst, J. *et al.* Mapping and analysis of chromatin state dynamics in nine human cell types. *Nature* **473**, 43-49, doi:10.1038/nature09906 (2011).

65 Scuderi, G. J. & Butcher, J. Naturally Engineered Maturation of Cardiomyocytes. *Front Cell Dev Biol* **5**, 50, doi:10.3389/fcell.2017.00050 (2017).

611 66 Hu, D. *et al.* Metabolic Maturation of Human Pluripotent Stem Cell-Derived
612 Cardiomyocytes by Inhibition of HIF1alpha and LDHA. *Circ Res* **123**, 1066-
613 1079, doi:10.1161/CIRCRESAHA.118.313249 (2018).
614 67 Gentillon, C. *et al.* Targeting HIF-1alpha in combination with PPARalpha
615 activation and postnatal factors promotes the metabolic maturation of human
616 induced pluripotent stem cell-derived cardiomyocytes. *J Mol Cell Cardiol* **132**,
617 120-135, doi:10.1016/j.yjmcc.2019.05.003 (2019).
618 68 Pinto, A. R. *et al.* Revisiting Cardiac Cellular Composition. *Circ Res* **118**, 400-
619 409, doi:10.1161/CIRCRESAHA.115.307778 (2016).
620 69 Ieda, M. *et al.* Cardiac fibroblasts regulate myocardial proliferation through
621 beta1 integrin signaling. *Dev Cell* **16**, 233-244,
622 doi:10.1016/j.devcel.2008.12.007 (2009).
623 70 Brutsaert, D. L. Cardiac endothelial-myocardial signaling: its role in cardiac
624 growth, contractile performance, and rhythmicity. *Physiol Rev* **83**, 59-115,
625 doi:10.1152/physrev.00017.2002 (2003).
626 71 Liu, R. *et al.* Tead1 is required for perinatal cardiomyocyte proliferation. *PLoS*
627 *One* **14**, e0212017, doi:10.1371/journal.pone.0212017 (2019).
628 72 Pikkarainen, S. *et al.* GATA-4 is a nuclear mediator of mechanical stretch-
629 activated hypertrophic program. *J Biol Chem* **278**, 23807-23816,
630 doi:10.1074/jbc.M302719200 (2003).
631 73 Xiang, F. L., Guo, M. & Yutzey, K. E. Overexpression of Tbx20 in Adult
632 Cardiomyocytes Promotes Proliferation and Improves Cardiac Function After
633 Myocardial Infarction. *Circulation* **133**, 1081-1092,
634 doi:10.1161/CIRCULATIONAHA.115.019357 (2016).
635 74 Wang, J., Liu, S., Heallen, T. & Martin, J. F. The Hippo pathway in the heart:
636 pivotal roles in development, disease, and regeneration. *Nat Rev Cardiol* **15**,
637 672-684, doi:10.1038/s41569-018-0063-3 (2018).
638 75 Kolodziejczyk, S. M. *et al.* MEF2 is upregulated during cardiac hypertrophy
639 and is required for normal post-natal growth of the myocardium. *Curr Biol* **9**,
640 1203-1206, doi:10.1016/S0960-9822(00)80027-5 (1999).
641 76 Ferdous, A. *et al.* FoxO1-Dio2 signaling axis governs cardiomyocyte thyroid
642 hormone metabolism and hypertrophic growth. *Nat Commun* **11**, 2551,
643 doi:10.1038/s41467-020-16345-y (2020).
644 77 Martin, O. J. *et al.* A role for peroxisome proliferator-activated receptor gamma
645 coactivator-1 in the control of mitochondrial dynamics during postnatal cardiac
646 growth. *Circ Res* **114**, 626-636, doi:10.1161/CIRCRESAHA.114.302562
647 (2014).

Figure legends

Figure 1. Comparative analysis of time-series transcriptomes from mouse hearts. Schematic of sample collection strategy from control and *cKO* mice for RNA-seq and time-ordered gene co-expression network (TO-GCN) analysis. **(B)** PCA plot of RNA-seq results. n=2 per group. **(C)** The TO-GCN structure with TF genes as nodes (blue circles) and the heatmap of average normalized RPKMs (z scores) at each time-point; TF genes were evaluated at nine levels in the control heart. Examples of TFs gene lists from each level in the control mice heart are shown. TFs shown at L1 and L2 were developmental cardiac associated, e.g., Gata4, Nkx2.5, Tbx5, Tbx20 and Tead1, in line with their known contributions to neonatal cell proliferation and maturation[71-73] (Supplementary file 1). The YAP co-factors (Smad3, Runx1, Smad4/5) shown at L3 and L4 (P7), consistent with their roles in the cardiac homeostasis and cell cycle control at postnatal stages[74]. The postnatal activation of Mef2 family (shown at L5 and L7) is required for normal postnatal growth of the myocardium[75], and Foxo1 (shown at L6) is necessary for hypertrophic growth[76]. The PPARs shown at L8 is responsible for mitochondria biogenesis and metabolic switching of CMs[77]. **(D)** KEGG analysis for co-expressed genes in the control heart are displayed in order (by TO-GCN level); the same list from *cKO* heart is shown for comparison.

Figure 2 Depletion of RNF20 before and after chamber formation leads to different outcomes.

(A) Experimental design for the generation and identification of heart-specific *Rnf20* conditional knockout mice at different developmental stages. Protein extracts were collected from the heart tube of *Rnf20*$^{flox/flox}$*;Mesp1-Cre* embryos (E10.5) and whole heart samples from *Rnf20*$^{flox/flox}$*;Mck-Cre* mice (P35); immunoblot analyses were performed **(B)** Growth curve and **(C)** Kaplan-Meier survival curves of *Rnf20 cKO* (*Rnf20*$^{flox/flox}$*;Mck-Cre*) mice and control (*Rnf20*$^{flox/flox}$, *Rnf20*$^{flox/+}$, *Mck-Cre Rnf20*$^{flox/+}$) littermates. **(D)** Hematoxylin/eosin-stained sagittal (left) and cross (right) sections of control (*Rnf20*$^{flox/flox}$) and *Rnf20 cKO* hearts at P2, P14, P28 and P42. **(E)** (Left panel) Representative 2D and M-mode echocardiographic images of the *RNF20 cKO* and control hearts. (Right panel) Echocardiographic analysis in the control and *cKO* mice at different stages. Left ventricular ejection fraction (EF) and fractional shortening (FS) are shown. Data are presented as mean ± SD; n=6 per group. * $p<0.05$; ** $p< 0.01$; *** $p< 0.001$. **(F)** Representative telemetric electrocardiogram (ECG) patterns of control and *cKO* mice at P14. Quantification of the ECG changes in *Rnf20 cKO* and control mice from P14 to P42 are shown; data are presented as mean ± SD. n=5 per group. * $p<0.05$; ** $p< 0.01$; *** $p< 0.001$.

Figure 3. Postnatal maturation defects in *Rnf20 cKO* mice heart.

(A) Model of the dynamic formation of intercalated discs (IDs; composed of desmosome, gap junction and adherens junction) during cardiomyocyte maturation. **(B)** Confocal micrographs of cross sections of the cardiac muscle of control and cKO mice at P2, P21 and P35. Specific antibodies were used to identify the distributions of ID component, N-Cadherin, and the costamere marker, Vinculin. The nucleus was visualized by Hoechst 33342 staining; n=3 per group. Scale bar: 10 μm. **(C)** Transmission electron microscopy images (TEMs) of ventricular myocardium from *Rnf20 cKO* and control mice at P21 and P35. The inset provides a simple representation of ID morphologies in control and *cKO* mice. Abnormal structures were observed in mutant hearts, with widened gaps in the IDs. White arrowheads: adherent junctions; yellow arrowheads: desmosomes. Scale bar: 0.5 μm. **(D)** Model of the morphological changes in immature cardiomyocytes; increased size and altered organization of the contractile cytoskeleton. **(E)** Staining for Vinculin (costamere marker) in ventricular sections from *Rnf20 cKO* and control mice at P2, P21 and P35. Scale bar: 50 μm. **(F)** The ultrastructure of the sarcomere in cardiomyocytes of control and *Rnf20 cKO* mice. Abnormal Z-line (white arrowheads) and loose, distorted myofibrils (yellow arrowheads) were observed in *cKO* mice at P21 and P35. Scale bar: 0.5 μm. **(G)** Schematic depicts the maturation of mitochondria during CM maturation. **(H)** TEMs of mitochondria in ventricular cardiomyocytes (Scale bar: 0.5 μm). Quantification of number of cristae per μm suggested a significantly less dense cristae structure in *cKO* mice heart than in control at P35 ($n = 3$ for each group). * $p<0.05$; ** $p< 0.01$; *** $p< 0.001$. **(I)** Immunoblotting for mitochondria proteins in control and *Rnf20 cKO* hearts (n=3). COX IV: cytochrome c oxidase IV; VDAC: voltage-dependent anion channel; PHB1: prohibitins; PDH: pyruvate dehydrogenase; SDHA: succinate dehydrogenase A; HSP60: heat shock protein 60. **(J-L)** The mitochondrial enzyme activities for (J) cytochrome c oxidase, (K) NADH oxidase and (L) ATP production were measured in P35 hearts ($n = 3$ for each, normalized to mitochondrial protein). * $p<0.05$; ** $p< 0.01$; *** $p< 0.001$.

Figure 4. Chromatin accessibility landscape in postnatal heart.

(A) Experimental design for sample collection from control and *cKO* mice. **(B)** Peak calls from the P7 and P21 control or mutant hearts are shown individually. Color indicates the type of genomic region overlapped by the peak. UTR, untranslated region. **(C)** Immunoblot analysis of RNF20 in control heart. **(D)** Venn diagram of peak-associated genes in the control and *Rnf20 cKO* heart at P7 (**Left**) and P21 (**Right**), respectively. **Middle,** model of peak associated genes from ATAC-seq (3 kb ± transcription start site). **(E)** Schematic illustrates the dynamics of TF binding (blue),

Tn5 insertion (green), and the concept of footprint analysis using ATAC-seq data. **(F)** Pairwise comparisons of TF activities in control and *cKO* mice. The volcano plots show differential binding activity versus -$\log_{10}$ p-value (both calculated by TOBIAS) for all investigated TF motifs; each dot represents one motif. The control-specific TFs (RNF20-dependent) are labeled in red, and the *cKO*-specific TFs (*cKO*-dependent) are labeled in blue. Gene ontology analyses of RNF20-dependent and *cKO*-dependent TFs are shown. **(G)** Illustration of RNF20-mediated chromatin remodeling in postnatal heart. At P7: RNF20 is upregulated, chromatin accessibility at regulatory elements (REs) of genes are upregulated, TF binding is upregulated; at P21: RNF20 is downregulated, chromatin accessibility at REs of genes are downregulated, TF binding is downregulated.

Figure 5. Working model.

(A) Schematic summarizes the effects of *Rnf20* inactivation (*cKO*) on mice heart development. **(B)** Dynamic RNF20 expression after birth mediates remodeling of chromatin accessibility to allow the induction of a time-ordered postnatal transcription program. RNF20 is highly expressed at the early postnatal stage, leading to a global chromatin decompaction that facilitates the binding of transcription factors (TFs) to early postnatal genes. RNF20 level decreases at the later stage of heart maturation, leading to chromatin compaction and a restriction of TF binding that establishes and maintains the mature status of the heart.

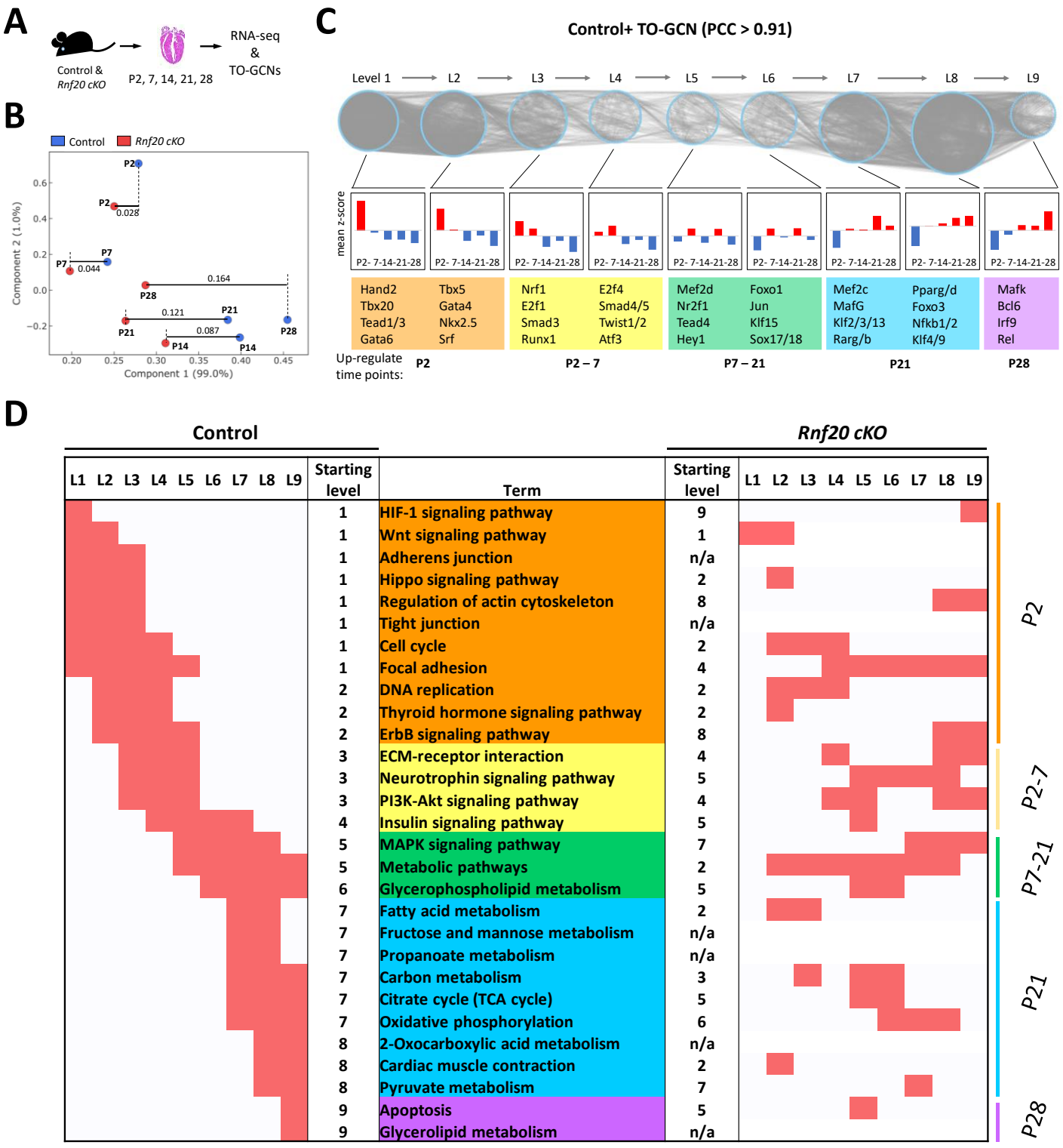
A
Control &
Rnf20 cKO
P2, 7, 14, 21, 28
RNA-seq
&
TO-GCNs
B
Control
Rnf20 cKO
Component 2 (1.0%)
Component 1 (99.0%)
P2
P7
P14
P21
P28
0.028
0.044
0.164
0.121
0.087
C
Control+ TO-GCN (PCC > 0.91)
Level 1
L2
L3
L4
L5
L6
L7
L8
L9
mean z-score
P2- 7-14-21-28
Hand2 Tbx5
Tbx20 Gata4
Tead1/3 Nkx2.5
Gata6 Srf
Nrf1 E2f4
E2f1 Smad4/5
Smad3 Twist1/2
Runx1 Atf3
Mef2d Foxo1
Nr2f1 Jun
Tead4 Klf15
Hey1 Sox17/18
Mef2c Pparg/d
MafG Foxo3
Klf2/3/13 Nfkb1/2
Rarg/b Klf4/9
Mafk
Bcl6
Irf9
Rel
Up-regulate time points:
P2
P2 – 7
P7 – 21
P21
P28
D
Control
Rnf20 cKO
L1 L2 L3 L4 L5 L6 L7 L8 L9
Starting level
Term
HIF-1 signaling pathway
Wnt signaling pathway
Adherens junction
Hippo signaling pathway
Regulation of actin cytoskeleton
Tight junction
Cell cycle
Focal adhesion
DNA replication
Thyroid hormone signaling pathway
ErbB signaling pathway
ECM-receptor interaction
Neurotrophin signaling pathway
PI3K-Akt signaling pathway
Insulin signaling pathway
MAPK signaling pathway
Metabolic pathways
Glycerophospholipid metabolism
Fatty acid metabolism
Fructose and mannose metabolism
Propanoate metabolism
Carbon metabolism
Citrate cycle (TCA cycle)
Oxidative phosphorylation
2-Oxocarboxylic acid metabolism
Cardiac muscle contraction
Pyruvate metabolism
Apoptosis
Glycerolipid metabolism
P2
P2-7
P7-21
P21
P28

Figure 1

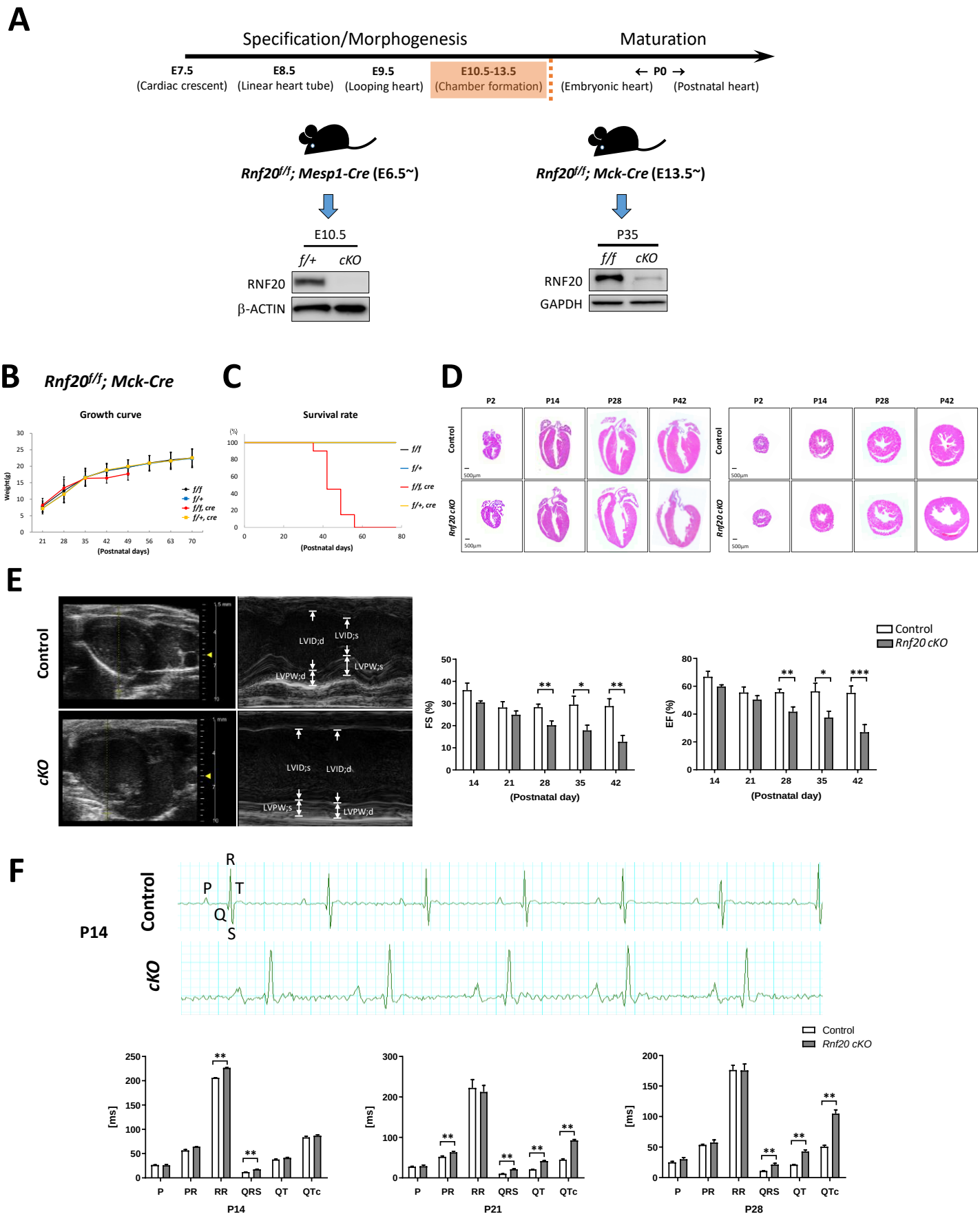
A
Specification/Morphogenesis
Maturation
E7.5
(Cardiac crescent)
E8.5
(Linear heart tube)
E9.5
(Looping heart)
E10.5-13.5
(Chamber formation)
← P0 →
(Embryonic heart)
(Postnatal heart)
Rnf20f/f; Mesp1-Cre (E6.5~)
Rnf20f/f; Mck-Cre (E13.5~)
E10.5
f/+
cKO
RNF20
β-ACTIN
P35
f/f
cKO
RNF20
GAPDH
B
Rnf20f/f; Mck-Cre
Growth curve
Weight(g)
(Postnatal days)
f/f
f/+
f/f, cre
f/+, cre
C
Survival rate
(%)
(Postnatal days)
f/f
f/+
f/f, cre
f/+, cre
D
P2
P14
P28
P42
Control
Rnf20 cKO
500μm
E
Control
cKO
LVID;d
LVID;s
LVPW;s
LVPW;d
FS (%)
EF (%)
(Postnatal day)
Control
Rnf20 cKO
F
P14
Control
cKO
R
P
T
Q
S
[ms]
P
PR
RR
QRS
QT
QTc
P14
P21
P28
Control
Rnf20 cKO

Figure 2

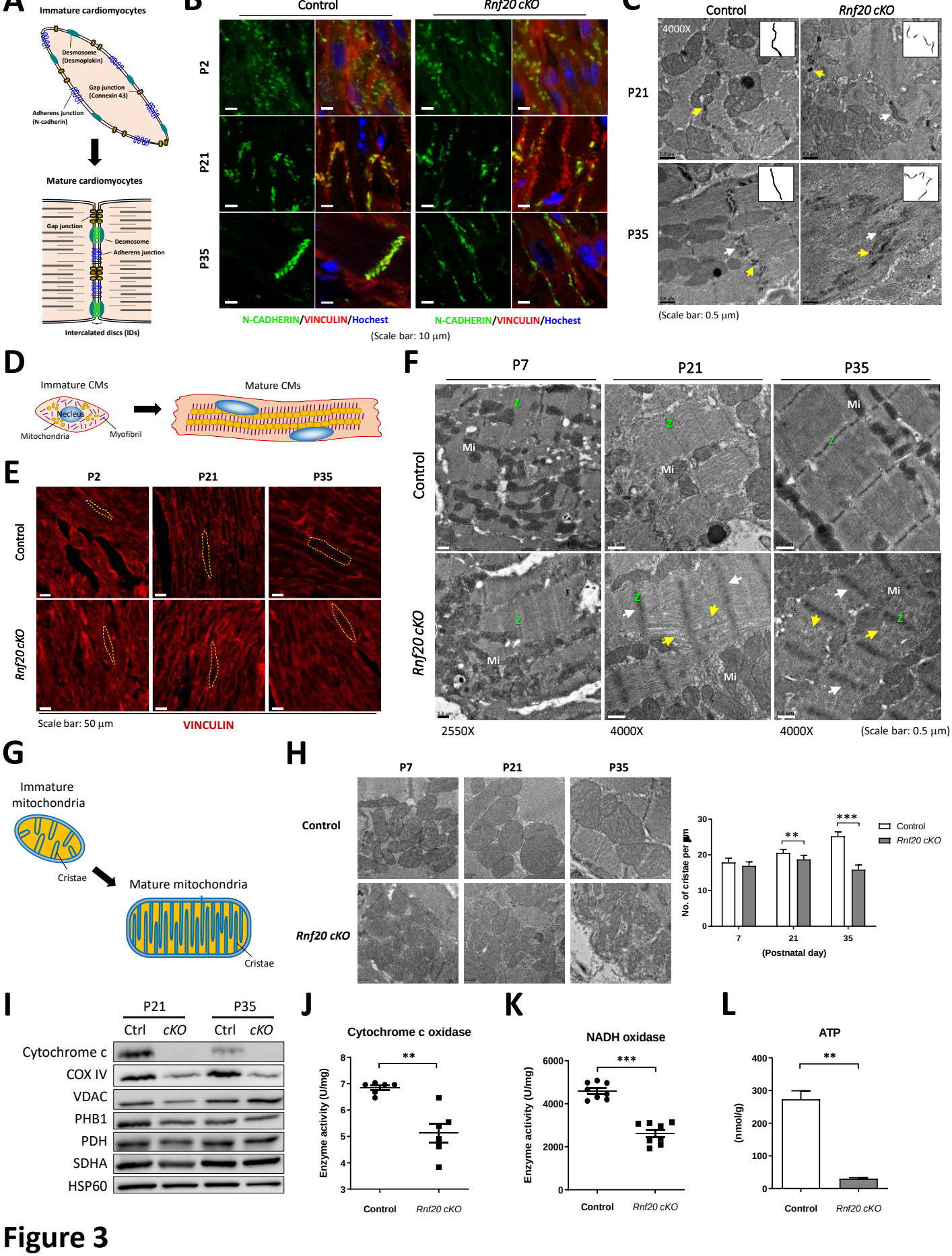
A
Immature cardiomyocytes
Desmosome (Desmoplakin)
Gap junction (Connexin 43)
Adherens junction (N-cadherin)
Mature cardiomyocytes
Gap junction
Desmosome
Adherens junction
Intercalated discs (IDs)
B
Control
Rnf20 cKO
P2
P21
P35
N-CADHERIN/VINCULIN/Hochest
N-CADHERIN/VINCULIN/Hochest
(Scale bar: 10 μm)
C
Control
Rnf20 cKO
4000X
P21
P35
(Scale bar: 0.5 μm)
D
Immature CMs
Mature CMs
Nucleus
Mitochondria
Myofibril
E
P2
P21
P35
Control
Rnf20 cKO
Scale bar: 50 μm
VINCULIN
F
P7
P21
P35
Control
Rnf20 cKO
Z
Mi
2550X
4000X
4000X
(Scale bar: 0.5 μm)
G
Immature mitochondria
Cristae
Mature mitochondria
Cristae
H
P7
P21
P35
Control
Rnf20 cKO
No. of cristae per μm
Control
Rnf20 cKO
(Postnatal day)
I
P21
P35
Ctrl
cKO
Ctrl
cKO
Cytochrome c
COX IV
VDAC
PHB1
PDH
SDHA
HSP60
J
Cytochrome c oxidase
Enzyme activity (U/mg)
Control
Rnf20 cKO
K
NADH oxidase
Enzyme activity (U/mg)
Control
Rnf20 cKO
L
ATP
(nmol/g)
Control
Rnf20 cKO

Figure 3

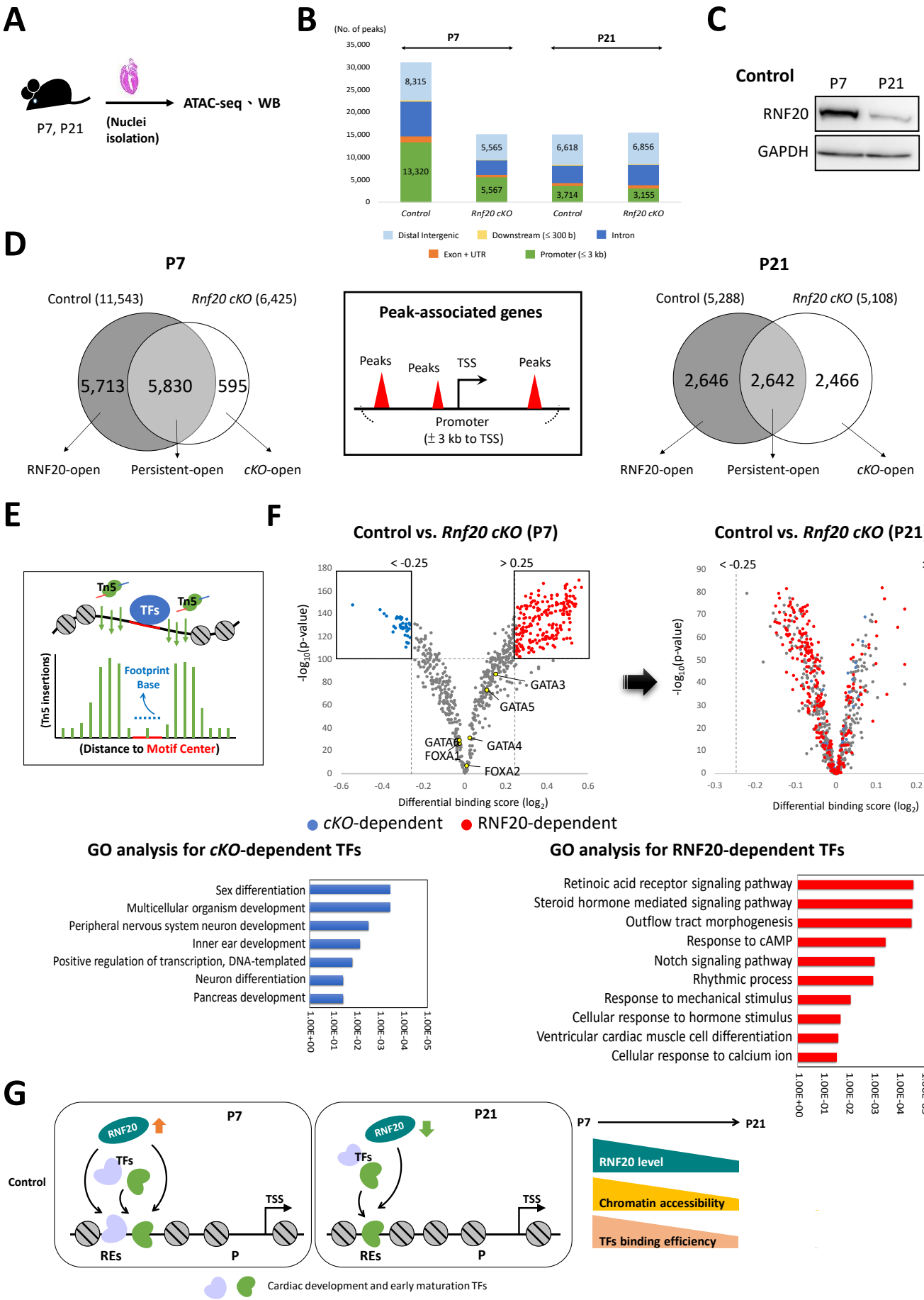
A
P7, P21
(Nuclei isolation)
ATAC-seq、WB
B
(No. of peaks)
P7
P21
35,000
30,000
25,000
20,000
15,000
10,000
5,000
0
8,315
13,320
5,565
5,567
6,618
3,714
6,856
3,155
Control
Rnf20 cKO
Control
Rnf20 cKO
Distal Intergenic
Downstream (≤ 300 b)
Intron
Exon + UTR
Promoter (≤ 3 kb)
C
Control
P7
P21
RNF20
GAPDH
D
P7
Control (11,543)
Rnf20 cKO (6,425)
5,713
5,830
595
RNF20-open
Persistent-open
cKO-open
Peak-associated genes
Peaks
Peaks
TSS
Peaks
Promoter
(± 3 kb to TSS)
P21
Control (5,288)
Rnf20 cKO (5,108)
2,646
2,642
2,466
RNF20-open
Persistent-open
cKO-open
E
Tn5
Tn5
TFs
Footprint
Base
(Tn5 insertions)
(Distance to Motif Center)
F
Control vs. Rnf20 cKO (P7)
< -0.25
> 0.25
-log10(p-value)
GATA3
GATA5
GATA6
FOXA1
GATA4
FOXA2
Differential binding score (log2)
Control vs. Rnf20 cKO (P21)
< -0.25
> 0.25
-log10(p-value)
Differential binding score (log2)
cKO-dependent
RNF20-dependent
GO analysis for cKO-dependent TFs
Sex differentiation
Multicellular organism development
Peripheral nervous system neuron development
Inner ear development
Positive regulation of transcription, DNA-templated
Neuron differentiation
Pancreas development
1.00E+00
1.00E-01
1.00E-02
1.00E-03
1.00E-04
1.00E-05
GO analysis for RNF20-dependent TFs
Retinoic acid receptor signaling pathway
Steroid hormone mediated signaling pathway
Outflow tract morphogenesis
Response to cAMP
Notch signaling pathway
Rhythmic process
Response to mechanical stimulus
Cellular response to hormone stimulus
Ventricular cardiac muscle cell differentiation
Cellular response to calcium ion
1.00E+00
1.00E-01
1.00E-02
1.00E-03
1.00E-04
1.00E-05
G
Control
P7
RNF20
TFs
TSS
REs
P
P21
RNF20
TFs
TSS
REs
P
P7
P21
RNF20 level
Chromatin accessibility
TFs binding efficiency
Cardiac development and early maturation TFs

Figure 4

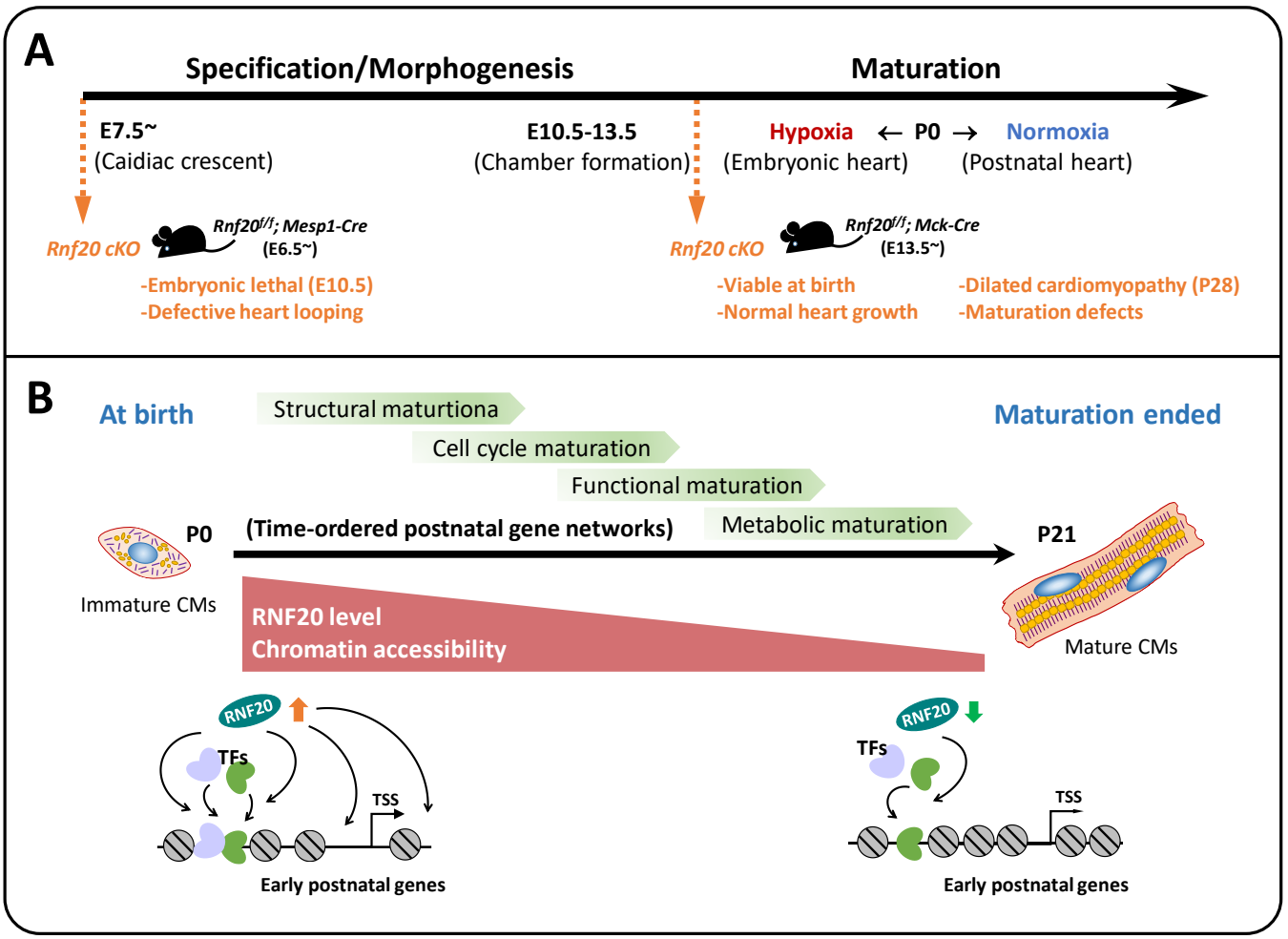
A
Specification/Morphogenesis
Maturation
E7.5~
(Caidiac crescent)
E10.5-13.5
(Chamber formation)
Hypoxia ← P0 → Normoxia
(Embryonic heart)
(Postnatal heart)
Rnf20 cKO
Rnf20f/f; Mesp1-Cre
(E6.5~)
-Embryonic lethal (E10.5)
-Defective heart looping
Rnf20 cKO
Rnf20f/f; Mck-Cre
(E13.5~)
-Viable at birth
-Normal heart growth
-Dilated cardiomyopathy (P28)
-Maturation defects
B
At birth
Structural maturtiona
Cell cycle maturation
Functional maturation
Metabolic maturation
Maturation ended
P0
(Time-ordered postnatal gene networks)
P21
Immature CMs
Mature CMs
RNF20 level
Chromatin accessibility
RNF20
TFs
TSS
Early postnatal genes
RNF20
TFs
TSS
Early postnatal genes

Figure 5